


RESEARCH PAPER

SPECIAL SERIES ON MITOCHONDRIAL BIOENERGETICS IN PHYSIOLOGY

Mitochondria can substitute for parvalbumin to lower cytosolic calcium levels in the murine fast skeletal muscle

Lorenzo Marcucci^{1,2}  | Leonardo Nogara¹ | Marta Canato¹ | Elena Germinario¹ | Anna Raffaello^{1,3} | Michela Carraro¹ | Paolo Bernardi¹ | Laura Pietrangelo^{4,5} | Simona Boncompagni^{4,6} | Feliciano Protasi^{4,5} | Nazareno Paolocci^{1,7} | Carlo Reggiani^{1,8}

¹Department of Biomedical Sciences, University of Padova, Padova, Italy

²Center for Biosystems Dynamics Research, RIKEN, Suita, Japan

³Myology Center, University of Padova, Padova, Italy

⁴CAST, Center for Advanced Studies and Technology, University G. d'Annunzio of Chieti-Pescara, Chieti, Italy

⁵DMSI, Department of Medicine and Aging Sciences, University G. d'Annunzio of Chieti-Pescara, Chieti, Italy

⁶DNICS, Department of Neuroscience and Clinical Sciences, University G. d'Annunzio of Chieti-Pescara, Chieti, Italy

⁷Division of Cardiology, The Johns Hopkins University School of Medicine, Baltimore, Maryland, USA

⁸Science and Research Center Koper, Institute for Kinesiology Research, Koper, Slovenia

Correspondence

Lorenzo Marcucci, Department of Biomedical Sciences, University of Padova, Padova, Italy.
Email: lorenzo.marcucci@unipd.it

Funding information

European Union via the Horizon 2020 Research and Innovation Programme under the Marie Skłodowska-Curie, Grant/Award Number: 886232; Italian Telethon Association, Grant/Award Number: GGP16026; Italian Ministry of Health, Grant/Award Number: GR-2016-02362779; Italian Ministry of University and Scientific Research, Grant/Award Number: PRIN 20207P85MH; Italian Telethon ONLUS, Grant/Award Number: GGP19231; National Institutes of Health USA, Grant/Award Number: AR059646

Abstract

Aim: Parvalbumin (PV) is a primary calcium buffer in mouse fast skeletal muscle fibers. Previous work showed that PV ablation has a limited impact on cytosolic Ca^{2+} ($[\text{Ca}^{2+}]_{\text{cyto}}$) transients and contractile response, while it enhances mitochondrial density and mitochondrial matrix-free calcium concentration ($[\text{Ca}^{2+}]_{\text{mito}}$). Here, we aimed to quantitatively test the hypothesis that mitochondria act to compensate for PV deficiency.

Methods: We determined the free Ca^{2+} redistribution during a 2 s 60 Hz tetanic stimulation in the sarcoplasmic reticulum, cytosol, and mitochondria. Via a reaction–diffusion Ca^{2+} model, we quantitatively evaluated mitochondrial uptake and storage capacity requirements to compensate for PV lack and analyzed possible extracellular export.

Results: $[\text{Ca}^{2+}]_{\text{mito}}$ during tetanic stimulation is greater in knock-out (KO) (1362 ± 392 nM) than in wild-type (WT) (855 ± 392 nM), $p < 0.05$. Under the assumption of a non-linear intramitochondrial buffering, the model predicts an accumulation of $725 \mu\text{moles}/L_{\text{fiber}}$ (buffering ratio 1:11 000) in KO, much higher than in WT ($137 \mu\text{moles}/L_{\text{fiber}}$, ratio 1:4500). The required transport rate via mitochondrial calcium uniporter (MCU) reaches 3 mM/s, compatible with available literature. TEM images of calcium entry units and Mn^{2+} quenching showed a

This is an open access article under the terms of the [Creative Commons Attribution](https://creativecommons.org/licenses/by/4.0/) License, which permits use, distribution and reproduction in any medium, provided the original work is properly cited.

© 2024 The Author(s). *Acta Physiologica* published by John Wiley & Sons Ltd on behalf of Scandinavian Physiological Society.

greater capacity of store-operated calcium entry in KO compared to WT. However, levels of $[Ca^{2+}]_{cyto}$ during tetanic stimulation were not modulated to variations of extracellular calcium.

Conclusions: The model-based analysis of experimentally determined calcium distribution during tetanic stimulation showed that mitochondria can act as a buffer to compensate for the lack of PV. This result contributes to a better understanding of mitochondria's role in modulating $[Ca^{2+}]_{cyto}$ in skeletal muscle fibers.

KEYWORDS

calcium, mitochondria, mouse skeletal muscle fibers, parvalbumin, reaction–diffusion model

1 | INTRODUCTION

In fast skeletal muscle fibers, the cytosolic-free Ca^{2+} concentration ($[Ca^{2+}]_{cyto}$) is finely tuned by the release and reuptake by the sarcoplasmic reticulum (SR), by the calcium-binding molecules, being troponin C (TnC) and parvalbumin (PV) the most prominent ones, and by the exchanges with the extracellular environment (see for a recent review¹). Parvalbumin is a high-affinity Ca^{2+} -binding protein found at high concentrations in vertebrates' fast-contracting/relaxing skeletal muscle.^{2,3} Following a Ca^{2+} release from SR, PV binds several hundred μ moles of calcium per fiber liter,^{4,5} hiding it from the Ca^{2+} sensors and significantly reducing the fluxes of Ca^{2+} to all other compartments and buffers. Notably, the increase in $[Ca^{2+}]_{cyto}$ following Ca^{2+} release⁶⁻⁸ or Ca^{2+} leakage^{9,10} from the SR is accompanied by a mitochondrial Ca^{2+} uptake in muscle fibers, as in most cell types. The increased Ca^{2+} concentration in the mitochondrial matrix enhances adenosine triphosphate (ATP) production.¹¹ In skeletal muscles, mitochondrial Ca^{2+} uptake also modulates fiber size.¹² High and prolonged Ca^{2+} uptake by mitochondria could trigger a permeability transition, leading to cell death.^{8,13} A more well-rounded appreciation of mitochondrial Ca^{2+} uptake in the skeletal muscle is warranted, including its potential contribution to modulating the amplitude of the $[Ca^{2+}]_{cyto}$ transient (as reviewed recently¹⁴). In this perspective, mice carrying a null mutation of the parvalbumin gene (PV-KO mice) represent an attractive model.

In a recent study,¹⁵ we showed increased Ca^{2+} uptake by mitochondria in PV-KO fibers compared to WT without any increase in cytosolic Ca^{2+} concentration. The increased intra-mitochondrial Ca^{2+} concentration ($[Ca^{2+}]_{mito}$) activated a signaling pathway leading to fiber hypertrophy. Mitochondrial density was also greater in PV-KO than in WT muscle fibers.

Based on our previous results,¹⁵ here we aim to quantitatively test the hypothesis that the enhanced

mitochondrial Ca^{2+} uptake can compensate PV lack in modulating $[Ca^{2+}]_{cyto}$. We selected the calcium release induced by submaximal tetanic stimulation (60 Hz for 2 s at 25°C), as a model. This protocol is sufficient to reach a steady state (fused tetanus and stable oscillations of $[Ca^{2+}]_{cyto}$) after 0.3 s of stimulation. We measured the redistribution of calcium in three compartments, namely cytosol, mitochondrial matrix, and lumen of the SR. The exchanges with extracellular space based on store-operated calcium entry (SOCE) and plasma membrane calcium ATPase (PMCA)/sodium calcium exchanger (NCX) were also evaluated. A reaction–diffusion model derived from that developed to study calsequestrin knock out (CSQ-KO) muscle fibers¹⁶ was implemented to simulate the Ca^{2+} distribution in WT and PV-KO muscle fibers.

2 | RESULTS

2.1 | Free Ca^{2+} concentration in the cytosol and the sarcoplasmic reticulum at rest and during electrical stimulation

The experimental conditions (2 s electrical stimulation at 60 Hz at 25°C) were chosen because they led to the development of approximately 80% of the maximal force both in PV-KO and WT flexor digitorum brevis (FDB) muscles (see the force-frequency curve Figure 1A), indicating a similar amount of Ca^{2+} buffered by the TnC. After approximately 0.3 s stimulation, the force reached a steady level, and the Fura-2 ratio signal, a slow-high affinity dye, showed stable oscillations (Figure 1B). We focused on the steady-state conditions and neglected the kinetics of the first initial phase (Figure 1C) and of the decay phase at the stimuli train's end, already analyzed in our previous study.¹⁵ During the steady-state phase of stimulation, the peak and the slope averaged over a high number of individual transients (Figure 1D,E) as well as the area under

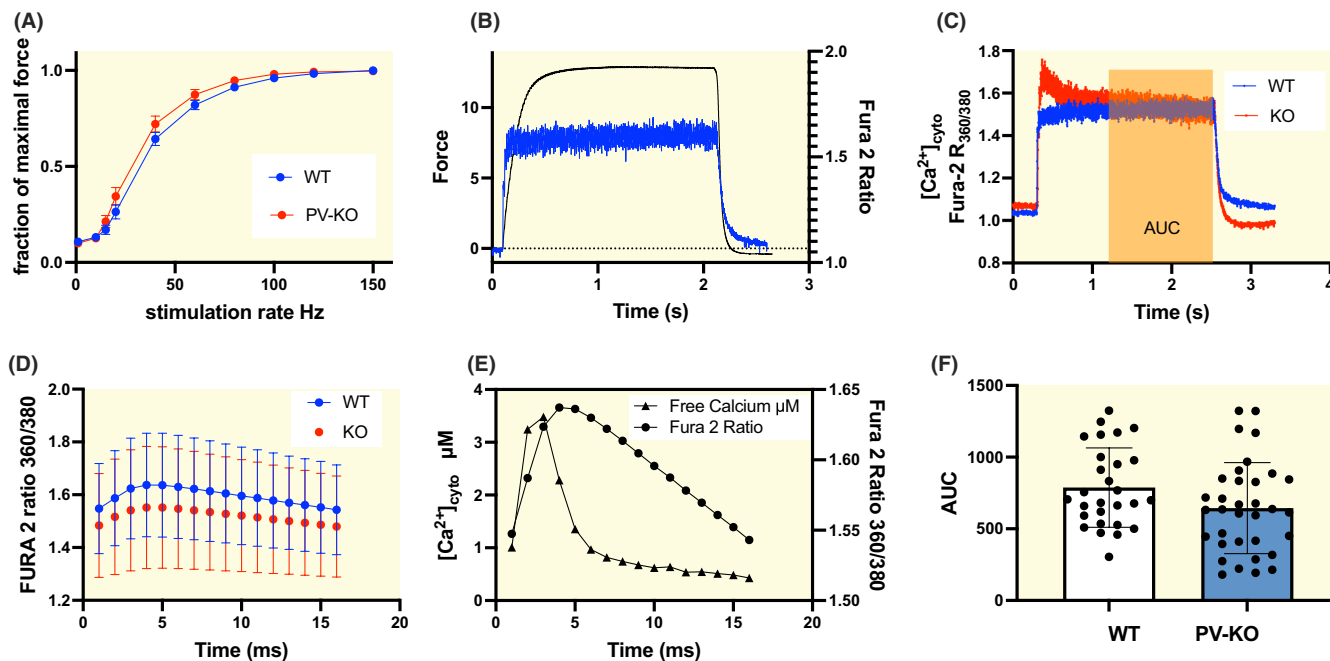


FIGURE 1 Characterization of 60 Hz, 2s tetanus. (A) Normalized force-frequency curve (2s tetani, 25°C, optimal length) of FDB muscles does not show a significant difference between WT and PV-KO ($n=10$ in each group). WT blue and PV-KO red. (B) Superimposed records of force development and Fura 2 ratio showing a cytosolic calcium transient during a 60 Hz, 2s tetanus. (C) Typical records of cytosolic calcium transient during a 60 Hz, 2s tetanus: WT blue and PV-KO red. The interval at steady state in which the area under Fura-2 curve (AUC) is calculated corresponds to 100 stimuli at 60 Hz and is indicated in the panel. (D) Averaged Fura-2 ratio in an individual response to electrical stimulus in the interval at steady state of the tetanus (average of 100 stimuli at 60 Hz, mean \pm SD). (E) Calculated cytosolic calcium concentrations in an individual response to electrical stimulus during the steady-state phase of the tetanus (2s, 60 Hz). (F) Statistical comparison between area under Fura-2 curve (AUC) in the region indicated in panel C does not show a significant difference ($p=0.066$) in WT versus PV-KO fibers. Each dot corresponds to a fiber.

the curve (Figure 1F) of the $[Ca^{2+}]_{cyto}$ as determined by Fura-2 ratio were not significantly different between PV-KO and WT.

Next, we analyzed the SR-free $[Ca^{2+}]$ ($[Ca^{2+}]_{SR}$) via D1-ER cameleon in quiescent fibers and during electrical stimulation. We did not observe significant variations between WT and PV-KO in the resting $[Ca^{2+}]_{SR}$, or in its decline during the train of stimuli (Figure 2).

2.2 | Mitochondrial Ca^{2+} uptake increased in the absence of PV

We previously showed that the concentrations of Ca^{2+} in the mitochondrial matrix ($[Ca^{2+}]_{mito}$) during a caffeine-induced Ca^{2+} release were significantly higher in PV-KO fibers.¹⁵ Here, we first analyzed the effect of parvalbumin ablation on mitochondrial metabolic function through the oxygen consumption rate and calcium retention capacity, and no statistical significance on the differences was achieved by either protocol (Figure S1). Next, we determined $[Ca^{2+}]_{mito}$ in FDB fibers at rest and during stimulation, expressed in nmol/ L_{mito} , measuring the ratio (R_{mito}) of the YFP and CFP intensities of the 4mtD3cpv sensor

(Figure 3). $[Ca^{2+}]_{mito}$ was significantly higher in PV-KO than in WT (Figure 3D–F) at rest and the peak of the tetanic stimulation. Instead, the rising rates at the onset of the stimuli (Figure 3B) and the decay rates at the end of stimulation (Figure 3C) did not show statistically significant differences between WT and PV-KO fibers.

Previous studies showed that mitochondrial density and size are greater in PV-KO than in WT,^{15,17,18} leading to a higher fraction of fiber volume occupied by mitochondria. Moreover, PV ablation increased the number of mitochondria coupled with the Ca^{2+} release units (CRU) (from 32.7 to 39.3 per 100 μm^2 in WT and PV-KO, respectively¹⁵), indicating, on average, a shift toward a microdomain with a higher Ca^{2+} concentration. Here, we found a slightly decreased density of Ca^{2+} release (CRUs or triads) in PV-KO fibers versus WT (Figure 4A,B and Table 1, column A).

To assess whether the increase further attests to the mitochondria's role in regulating the $[Ca^{2+}]_{cyto}$ during 60 Hz stimulation, we tried to inhibit Ca^{2+} uptake via mitochondrial calcium uniporter (MCU). More specifically, in our previous work, we reported¹⁵ that MCU silencing increased the $[Ca^{2+}]_{cyto}$ upon the large Ca^{2+} release induced by caffeine. Here, we tested whether depression of Ca^{2+} uptake via MCU could affect $[Ca^{2+}]_{cyto}$ during 60 Hz

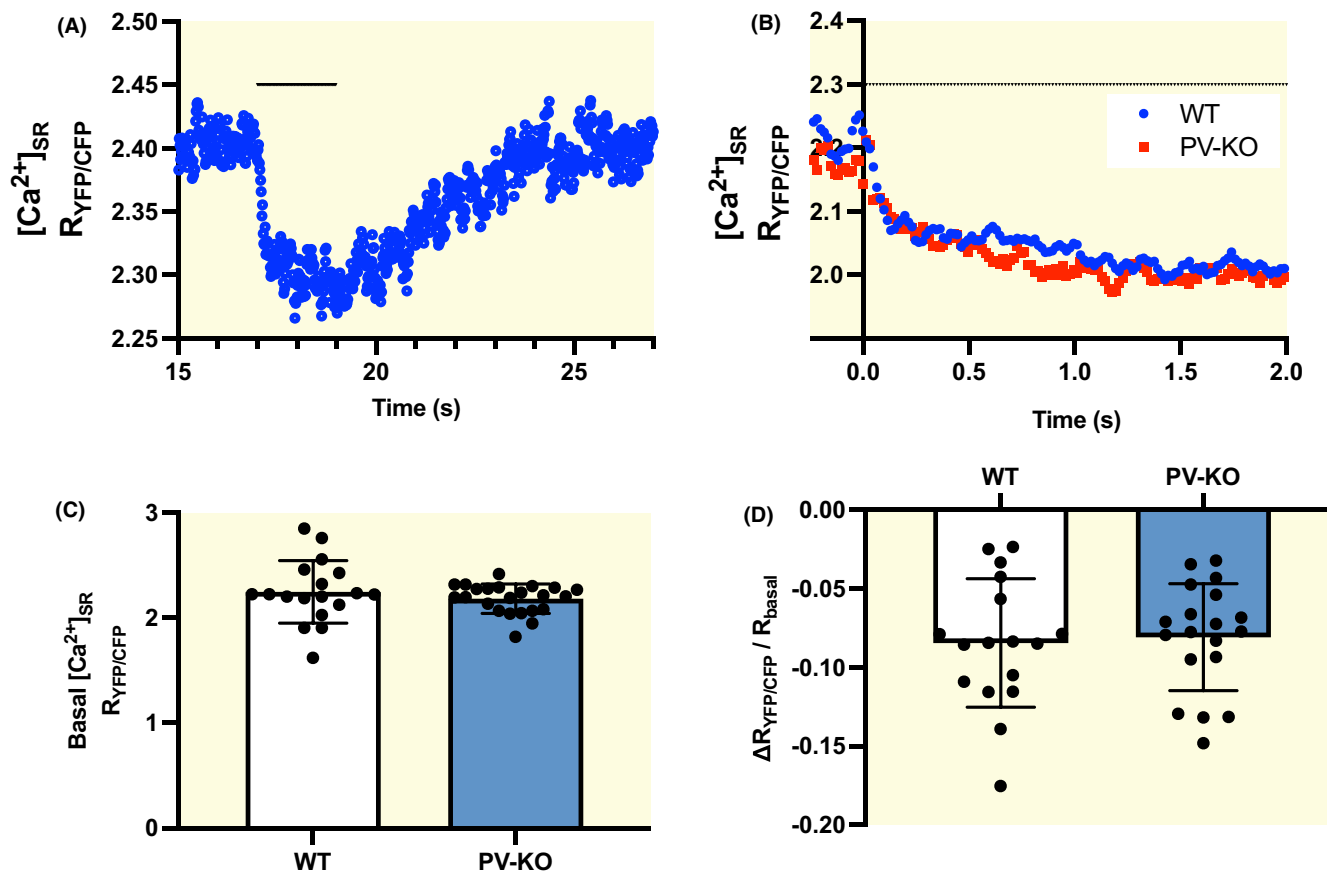


FIGURE 2 Free Ca^{2+} concentration in sarcoplasmic reticulum detected with cameleon D1-ER. (A) Typical-free Ca^{2+} concentration transient detected with cameleon D1-ER during 2s stimulation at 60 Hz. Stimulation interval indicated by a black segment. (B) Average of the decrease phase in WT ($n=17$) and PV-KO ($n=16$) fibers, WT blue and PV-KO red. Stimulation interval indicated by a black segment. (C) Basal values of D1-ER ratio at rest, means, and SD ($p=0.26$). (D) Fractional decrease in D1-ER ratio during a transient induced by 2s 60 Hz electrical stimulation, means, and SD ($p=0.55$).

stimulation. To this end, we followed two alternatives: (i) silencing via plasmid transfection and (ii) the use of a novel MCU inhibitor (MCU-i11²⁰). Both protocols did not yield a statistically significant conclusion (Figure S2A,B), likely due to the limited Ca^{2+} release lower than in the caffeine test, the only partial depression of MCU function, and high variability of the results. Numerical simulations (see below) confirmed that, without a complete MCU inhibition, the steady $[Ca^{2+}]_{cyto}$ during tetanic stimulation will be only marginally affected (Figure S2C,D).

2.3 | Extracellular Ca^{2+} fluxes in the absence of PV

EM analysis (Figure 4A,B) also revealed a higher incidence of fibers presenting SR-stacks and the number of SR-stacks inside those fibers in PV-KO fibers versus WT (Table 1, columns B and C). SR-stacks are assumed to be the main component of Ca^{2+} entry units (CEUs) involved in SOCE.^{19,21} Besides, TT network (Table 1, columns D

and E), that is, the second component of CEUs, showed that the total TT length/100 μm^2 and TT/SR-stack contact length increased in PV-KO.

Next, to establish the functional relevance of greater CEU presence, we measured the rate of Mn^{2+} quenching of Fura-2 fluorescence in WT and PV-KO FDB fibers after SR depletion. Interestingly, the quenching rate increases by 1.6 times in PV-KO just as the SR-stack density (Figure 4C,D). However, no significant differences in $[Ca^{2+}]_{cyto}$ transient (area under the curve at steady state) were detectable between WT and PV-KO fibers in the presence and absence of the external Ca^{2+} (see Figure S3).

2.4 | Calcium distribution at rest and during tetanus estimated in a mathematical model of Ca^{2+} diffusion

We improved our previously published rotational symmetric half-sarcomere model,¹⁶ based on three main compartments: mitochondria, cytosol, and SR (see Figure 5)

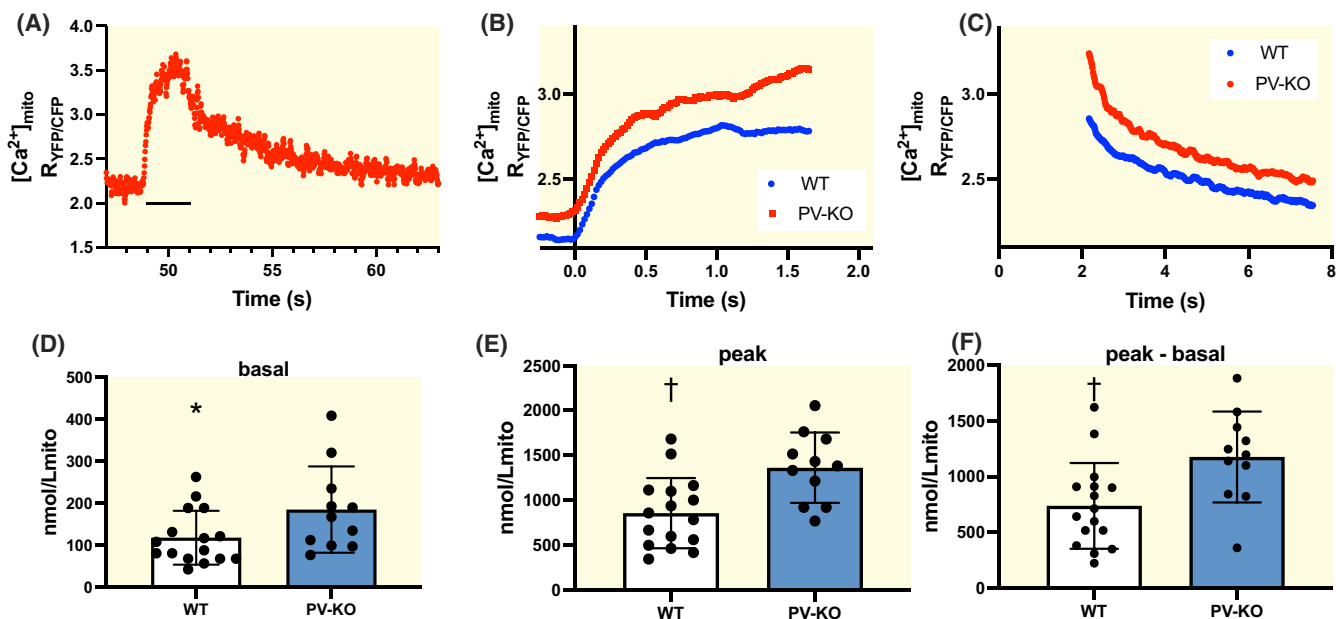


FIGURE 3 Free Ca^{2+} concentration in mitochondrial matrix detected with the 4mtD3cpv cameleon. (A) Typical-free Ca^{2+} transient detected as $R_{YFP/CFP}$ in the mitochondrial matrix. Stimulation interval indicated by a black segment. (B) Average (WT $n=13$ WT, PV-KO $n=9$) of the rising phase of $R_{YFP/CFP}$. Interpolation with an exponential function did not show statistically significant differences in the rising rate between WT (blue) and PV-KO (red), $p=0.38$. (C) Average (WT $n=13$ WT PV-KO $n=9$) of the decay phase of $R_{YFP/CFP}$. Interpolation with an exponential function did not show statistically significant differences in the decay rate between WT (blue) and PV-KO (red), $p=0.14$. (D) $[Ca^{2+}]_{mito}$ basal at rest in nmol/L, (WT: 118.3 ± 63.9 , $n=16$, PV-KO: 185.2 ± 103 , $n=11$, mean values and SD, $*p=0.0467$). (E) $[Ca^{2+}]_{mito}$ peak value reached during 2 s 60 Hz electrical stimulation in nmol/L, (WT: 855 ± 392 , $n=16$, PV-KO: 1362 ± 392 , $n=11$, mean values and SD, $^{\dagger}p=0.0029$). (F) $[Ca^{2+}]_{mito}$ (peak-basal) in nmol/L (WT: 737 ± 385 , $n=16$, PV-KO: 1177 ± 410 , $n=11$, mean values and SD, $^{\dagger}p=0.0088$).

to properly account for the local $[Ca^{2+}]_{cyto}$ around mitochondria (microdomains) and the inferred modifications of the average distances of the mitochondria from the ryanodine receptor (RyR) in WT and PV-KO fibers. Based on the assumed total length $L=1.25 \mu m$ and radius $R=0.5 \mu m$, $n=10$ radial and $m=20$ longitudinal compartments ($N_{compartments}=200$) (see Equations 1 in SI), allowed reaching the required precision of few tens of nanometers (see below). Also, we improved the original model (i) To specifically focus on the role of PV, associating this calcium buffer to a different variable for each compartment (SI Equation 2). (ii) To account for locally variable $[Mg^{2+}]_{cyto}$ which is a competitor of Ca^{2+} for PV. (iii) The influence of the Mg^{2+} on MCU^{22,23} has also been added (SI Equation 6), to reproduce the difference between the WT case, where $[Mg^{2+}]_{cyto}$ increases when Ca^{2+} binds to PV during stimulation and PV-KO case, where the $[Mg^{2+}]_{cyto}$ is assumed to be constant at rest and during stimulation. (iv) A cooperative mitochondrial buffer was introduced to reproduce the high ratio of bound-to-free calcium recently observed in skeletal muscle fibers.^{9,24,25} (v) Troponin has been implemented introducing two cooperative binding sites (SI Equation 3). (vi) NCX-like calcium transporter was added to simulate the flux toward the extracellular space in the T-tubule (SI Equation 7). Calsequestrin, RyR, and sarco-endoplasmic reticulum calcium ATPase

(SERCA) pumps characterizing the SR (SI Equations 4 and 5), and SOCE (SI Equation 8) are like the previous model. All the relevant equations are reported in the SI.

Using the model, we quantified the effect of PV ablation on Ca^{2+} handling in WT and PV-KO fiber (see Table 2 for the total calcium redistribution). Global (not local) $[Ca^{2+}]_{cyto}$ in the sole absence of PV, without any alternative buffering system, is predicted to be up to $60 \mu M$ during a 60 Hz 2 s tetanic stimulation (see supporting information Model). $[Ca^{2+}]_{cyto}$ determined with Fura-2 during the steady-state phase of tetanic stimulation was $3.5 \mu M$ (see Figure 1E), and such a huge $[Ca^{2+}]_{cyto}$ increase was never found by experimental data. Thus, we asked the model to indicate an alternative mechanism that can handle the Ca^{2+} ions with similar (i) amounts and (ii) rates as PV.

(i) Concerning the mitochondrial Ca^{2+} storage, our experimental records of $[Ca^{2+}]_{mito}$ with cameleon 4mtD3cpv (see Figure 3) and their calibration (see Figure S5) show an increase in the free $[Ca^{2+}]_{mito}$, in PV-KO fibers compared to WT of about $0.5 \mu mol/L_{mito}$ or (assuming the mitochondria volume is 5% of fiber volume) $25 nmol/L_{fiber}$ in WT fibers. Associating it to the total/free ratio of 5000:1, recently reported⁹ in quiescent WT skeletal muscle mitochondria, the extra-amount stored in the mitochondria in PV-KO

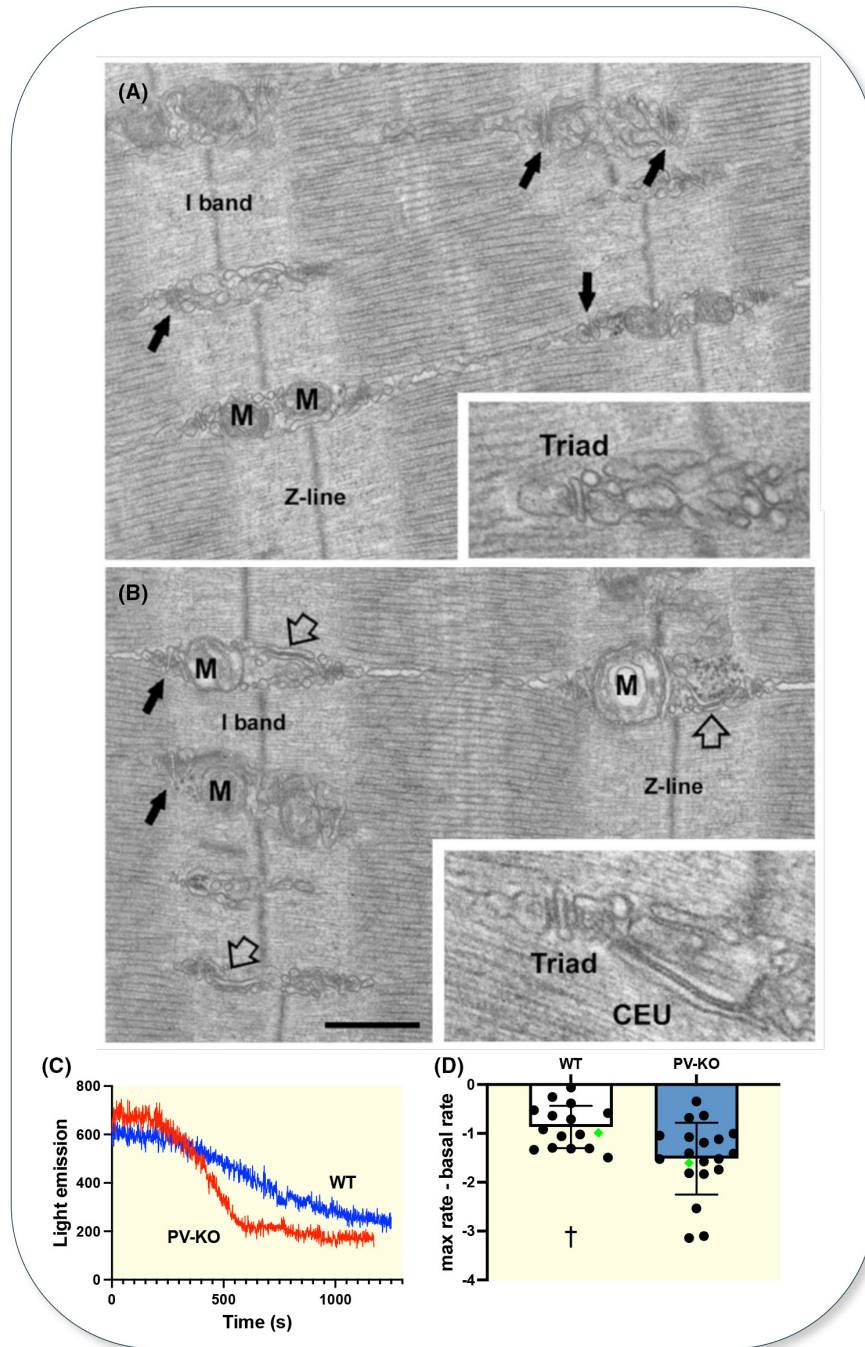


FIGURE 4 Quantitative analysis of Ca^{2+} release units (CRUs or triads) and Ca^{2+} entry units (CEUs). (A and B) Representative longitudinal electron microscopy (EM) images showing of Ca^{2+} release units (CRUs or triads) and Ca^{2+} entry units (CEUs) in adult fiber from WT and PV-KO mice. (A) A portion of fiber from adult WT mouse in longitudinal section, with CRUs positioned at the I-A band transition of the sarcomere (small black arrows), often found on both sides of the Z-line and in the proximity of mitochondria (M). Inset: Enlargement of a CRU. (B) CRUs in fibers of PV-KO mice are distributed as in WT fibers (small black arrows). The empty arrows point to membranes within the I band that are rearranged into SR stacks. Inset: Higher magnification of SR stack near a triad. Scale bars: A and B, $0.5\ \mu\text{m}$; insets, $0.2\ \mu\text{m}$. (C and D) *SOCE* rate in PV-KO compared to WT. (C) Recording of Mn^{2+} quenching on Fura-2 fluorescence in FDB fibers loaded with Fura-2, fully depleted by incubation and exposed to Ca^{2+} -free medium supplemented with $0.5\ \text{mM}$ MnCl_2 , WT blue and PV-KO red. (D) Maximal rate of fluorescence quenching expressed as a difference to the basal initial rate $R_{\text{SOCE}} = R_{\text{max}} - R_{\text{baseline}}$ (WT: -0.87 ± 0.43 , $n=16$, PV-KO: -1.52 ± 0.73 , $n=20$, mean values and SD, $^\dagger p=0.007$). Each dot corresponds to a fiber. Green symbols refer to the traces shown in C.

TABLE 1 Quantitative analysis of calcium release units (CRUs or triads) and calcium entry units (CEUs).

	A	B	C	D	E
	N. of CRUs/ $100\ \mu\text{m}^2$	Fibers with SR-stacks, % of total	N. of SR-stacks/ $100\ \mu\text{m}^2$	T Tubule length (μm)/ $100\ \mu\text{m}^2$	TT/SR contact length (μm)/ $100\ \mu\text{m}^2$
WT	79.2 ± 20.3	26.3 ± 11.5	2.1 ± 4.0	1.8 ± 5.5	0.7 ± 2.3
PV-KO	$71.8 \pm 17.2^{**}$	$77.3 \pm 3.1^{**}$	$4.0 \pm 4.5^*$	$2.8 \pm 3.5^*$	$2.3 \pm 3.2^{**}$

Note: Column A: Quantitative analysis of n. of CRUs/area reported as average number/ $100\ \mu\text{m}^2$. Column B and C: Percentage of fibers presenting SR-stacks and number of SR-stacks per area of section reported as the percentage of total fiber number and average stacks number/ $100\ \mu\text{m}^2$, respectively. Columns D and E: Total extension of the transverse tubule (TT) within the I band of sarcomere and length of TT adjacent to SR-stack membranes (i.e., TT/SR contact length) measured in transverse sections at 28.000X of magnification and reported as average (in μm)/ $100\ \mu\text{m}^2$.¹⁹ Sample size: 30 fibers from six WT mice; 30 fibers from three PV-KO mice.

** $p < 0.01$; * $p < 0.05$.

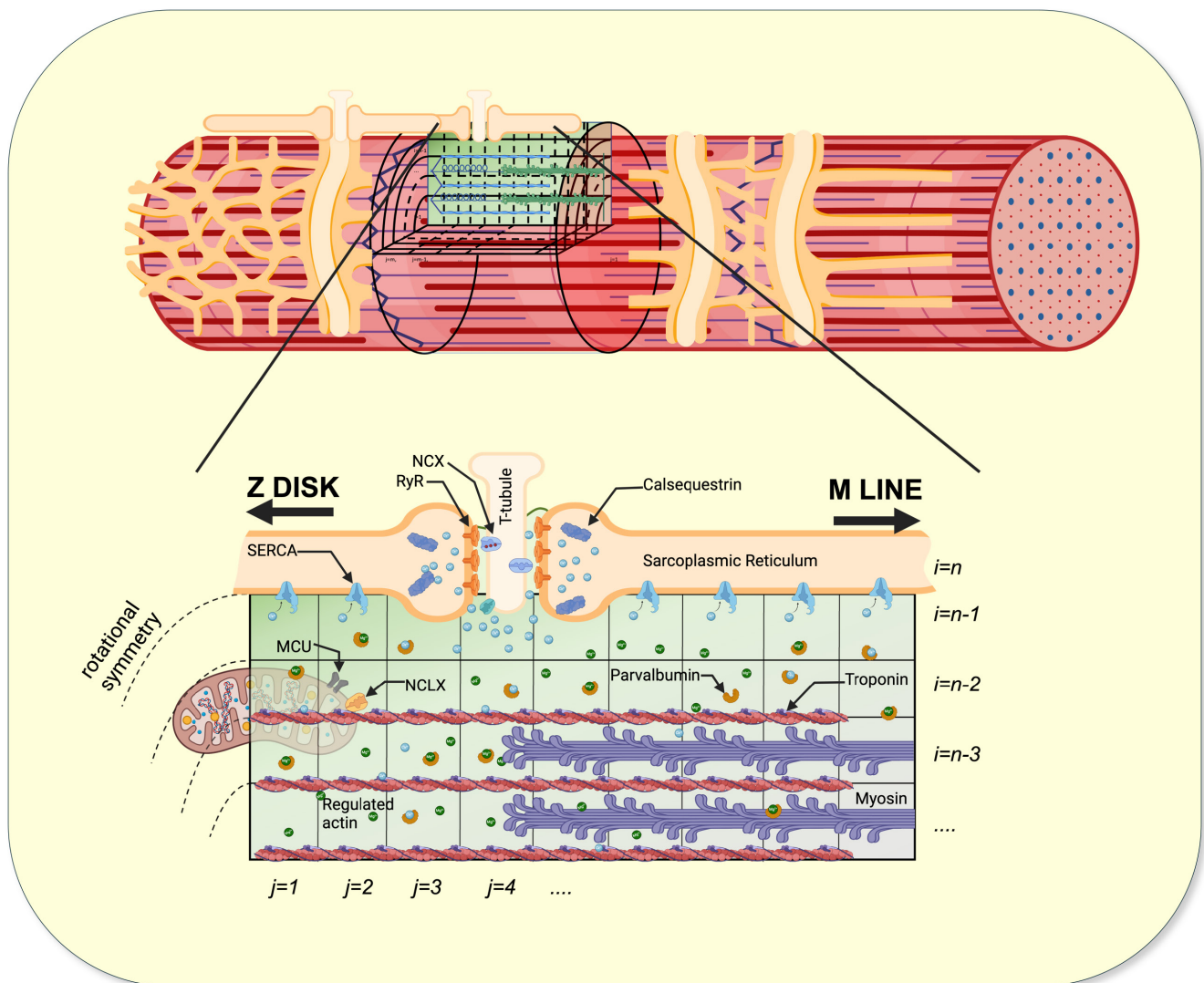


FIGURE 5 Multicompartmental reaction–diffusion model. Schematic view of the model reproducing a cylindrical half sarcomere (upper part), divided in $n = 10$ radial and $m = 20$ longitudinal compartments (only a part is shown in the figure where a part of the sarcomere is enlarged), to quantitatively simulate the free Ca^{2+} concentration in the various regions of the model. Based on the assumed total length $L = 1.25\ \mu\text{m}$ and radius $R = 0.5\ \mu\text{m}$, the values of m and n are chosen to simulate the observed details of the average distances of the mitochondria from the RyR in WT (160 nm) and PV-KO fibers (117 nm). Main structures, buffers, pumps, and channels are represented in the figure and described in Supporting information. Created with [BioRender.com](https://www.bio-render.com/).

TABLE 2 Model predictions of calcium distribution in different compartments at rest and during the steady-state phase in WT and PV-KO.

$\mu\text{moles}/L_{\text{fiber}}$	WT rest	WT act	Delta	PVKO rest	PVKO act	Delta
SR Total calcium	3209	2311	898	3209	2307	902
Bound to PV	318	893	575	–	–	–
Bound to Troponin	7	204	197	7	207	200
Mitochondria	21	137	116 (13% of Total)	29	725	696 (77% of Total)
Total calcium						

Note: Model predictions of calcium distribution in the sarcoplasmic reticulum (first row), buffered in the cytosol (second row, PV, third row TnC), and in the mitochondria (fourth row) at rest (first and fourth columns) and during the steady-state phase of tetanus (second and fifth columns, differences (delta) between rest and activity are reported in the third and sixth columns) in WT and PV-KO.

compared to WT fibers can reach $125 \mu\text{mol}/L_{\text{fiber}}$ in case of only linear buffering. The storage capacity increases further in our simulations where we assumed the cooperative mitochondria buffering system, as proposed by Bazil et al. 2013 for the cardiac muscle,²⁵ in the absence of experimental data on skeletal muscle. Notably, the bound-to-free ratio might increase for genetically modified muscle fiber.⁹ If we repeat the same calculation in PV-KO, the simulated total Ca^{2+} stored in mitochondria during stimulation will rise from about $137 \mu\text{mol}/L_{\text{fiber}}$ in WT to $725 \mu\text{mol}/L_{\text{fiber}}$ in PV-KO (Figure 6 and Table 2). Thus, the amount of Ca^{2+} entering the mitochondria under these hypotheses is likely sufficient to compensate for the lack of PV.

- (ii) The mitochondrial Ca^{2+} uptake kinetics is strictly related to their distance from the RyR, that is, from regions at higher $[\text{Ca}^{2+}]_{\text{cyto}}$. Our current and previous structural data (Table 1A and Figure 4E in Butera et al.¹⁵) indicate an average distance 20%–30% greater in WT than in PV-KO. Assuming the nearest distance of 130 nm between RyRs and mitochondria²⁶ for the PV-KO case, the WT case becomes 160 nm. Our model can modulate these parameters, varying the compartment in which MCU and sodium-calcium-lithium exchanger (NCLX) are localized. Despite the locally higher $[\text{Ca}^{2+}]_{\text{cyto}}$ the low value of the apparent Kd ($2 \mu\text{M}$ ²⁷) limits the increased Ca^{2+} uptake. However, in the model we included also the influence of the Mg^{2+} (not released from PV during Ca^{2+} transient in the PV-KO fibers) inhibition of the MCU, as observed experimentally on cardiac mitochondria.²² The model matches our data in both cases with a v_{MCU} flux of about $3 \text{mmoles}/L_{\text{fiber}}/\text{s}$, in WT, and about 43% higher in PV-KO. Interestingly, this value is close to the experimental determinations by Fieni and coworkers²⁸ and Yi and colleagues.²⁹ It is worth to note that the estimation of the amount of calcium entering the mitochondria depends only on the experimentally observed free $[\text{Ca}^{2+}]_{\text{mito}}$ and the imposed properties of

the mitochondrial buffer, regardless of the values of the $[\text{Ca}^{2+}]_{\text{cyto}}$. The values of free $[\text{Ca}^{2+}]_{\text{cyto}}$ in contracting skeletal muscle fibers are still debated, ranging from about 1^{30} to $10\text{--}15 \mu\text{M}$.^{4,5} If different values are imposed than what are used in this work, the MCU parameters in the model must be adjusted to assure the same maximal value of v_{MCU} flux required by mitochondrial storage.

Finally, we tested the possible contribution of Ca^{2+} flux toward the extracellular space. The differences in the potential transmembrane exchange between WT and PV-KO are derived directly from our data. In PV-KO fibers, under the assumption of an identical increase in both the extracellular efflux and the influx, both rates had to be increased by 70 times to obtain the observed $[\text{Ca}^{2+}]_{\text{cyto}}$ ($3.5 \mu\text{M}$) after 2 s of stimulation (Figure 7). Such an increment is much above the approximately two times increase in SOCE observed in our experiments.

3 | DISCUSSION AND CONCLUSIONS

Parvalbumin is a primary Ca^{2+} buffer in the cytosol of fast skeletal muscle fibers. Here, we demonstrate that an increase in mitochondrial density and calcium uptake can compensate for the lack of parvalbumin in cytosolic calcium modulation.

During Ca^{2+} release from SR, parvalbumin can bind more than $300 \mu\text{moles}/L_{\text{fiber}}$ Ca^{2+} , well above the $240 \mu\text{moles}/L_{\text{fiber}}$ that can be bound by the two Ca^{2+} binding sites of Troponin C.^{4,5} The complete ablation of PV in murine fast fibers does not create an excessive accumulation of Ca^{2+} in the cytosol but only minor alterations in the decay phase of the transient.^{15,31} The main adaptation of PV ablation is the increased mitochondrial density^{17,18} and, as shown in our previous study,¹⁵ an increased calcium uptake by mitochondria. The increased uptake is detectable both in constitutive knockout and

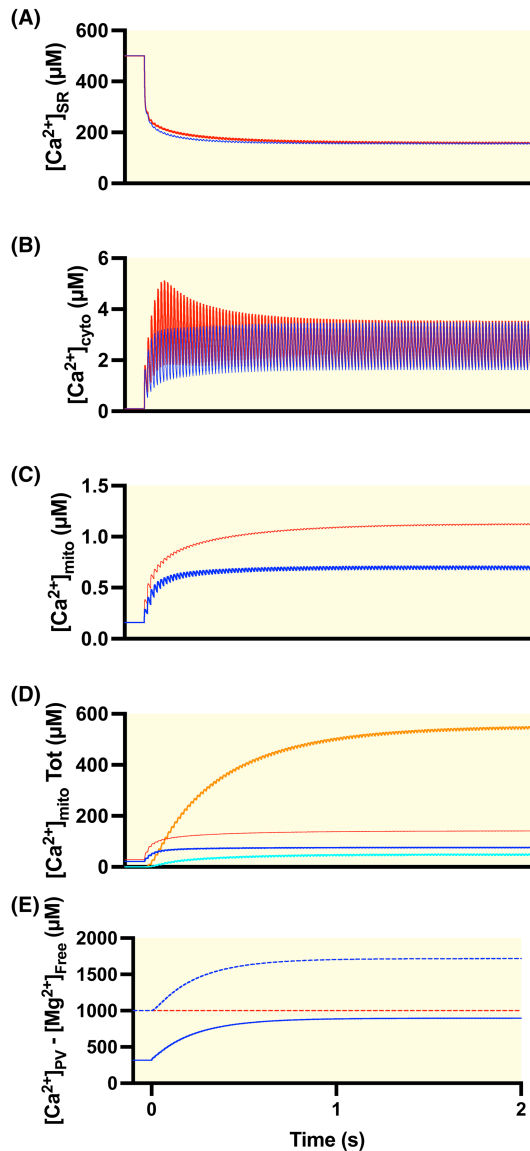


FIGURE 6 Model simulations of calcium redistribution during a 2 s, 60 Hz tetanus, showing the mitochondrial role. Free or total Ca^{2+} concentrations per L_{fiber} in WT (blue) and PV-KO (red) in the relevant compartments. In SR (A), basal level and depletion are similar in the two cases, as well as the cytosolic-free Ca^{2+} (B) in the steady state of the tetanic transient, fitting the experimental data. Free mitochondrial Ca^{2+} concentrations (C) closely reproduce the experimental values, and total mitochondrial Ca^{2+} concentrations (D) highlight the different roles of the low (blue and red for the WT and PV-KO, respectively) and of the high cooperative buffers (cyan and orange for the WT and PV-KO, respectively). The latter is able to balance, in the PV-KO case, the amount of Ca^{2+} not bounded by parvalbumin. Ca^{2+} bound to parvalbumin (blue continuous line, shown only in the WT case) and free Mg^{2+} (dashed lines, increasing in WT but constant in the PV-KO case) are shown in (E).

acute downregulation.¹⁵ Importantly, no change is detectable in fiber type marker expression as myosin or SERCA isoforms.^{15,31}

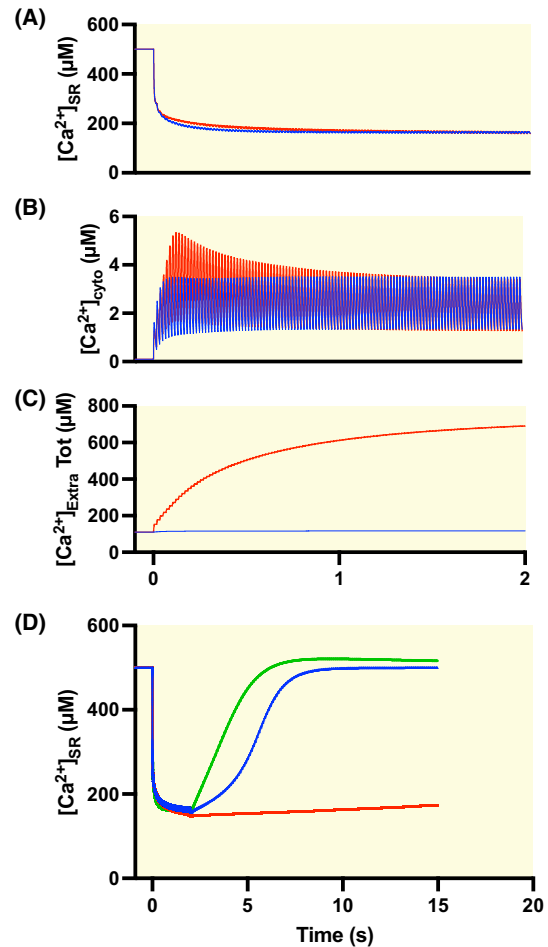


FIGURE 7 Model simulations of the impact of extracellular space exchanges. Free or total Ca^{2+} concentrations per L_{fiber} in WT (blue) and PV-KO (red) in the relevant compartments. In sarcoplasmic reticulum (A), basal level and depletion are set similar in PV-KO and WT. To fit the experimental data on the cytosolic-free Ca^{2+} (B) in the steady state, the total Ca^{2+} extruded toward the extracellular space (C) must be made comparable to the calcium not bound by PV. In the model, we reached this goal through a phenomenological exponential increase in the PMCA/NCX extrusion rate above a threshold in the $[\text{Ca}^{2+}]_{\text{cyto}}$ (red line, see supplementary information). Panel D shows (on a different time scale) the slow recovery of the free $[\text{Ca}^{2+}]_{\text{SR}}$ after the train of stimuli. In WT (blue) it is completed in a few seconds, while it is much slower in the PV-KO case when we increase the SOCE flux of factor 2, as observed experimentally (red). Only with a multiplicative factor of one order of magnitude higher (green) can the recovery be closer to the WT case, suggesting that this path is less important in the Ca^{2+} handling in PV-KO.

At variance with our previous work,¹⁵ where we analyzed several muscles of the mouse leg and induced calcium release with caffeine, we adopted as a model FDB and calcium release induced in a more physiological protocol of electrical stimulation.

FDB is a fast muscle composed mainly of 2A and 2X fibers,³²⁻³⁴ which are less rich in PV than fast 2B fibers but

definitely richer in mitochondria.³⁵ For two decades, FDB has become the standard reference for studying calcium signals in murine single muscle fibers. We adopted Fura-2 and two cameleons (ER-D1 and 4mtD3cpv) targeted to SR and mitochondria³⁶ to measure free calcium concentration. The choice ofameleon was based on our previous experience with those dyes.^{7,37,38} In particular, 4mtD3cpv has a low affinity (K_d in vivo $>2.5\mu\text{M}$, see Figure S5) and seems suitable to follow the mitochondrial calcium kinetics.^{7,39} The choice of Fura-2, a slow, high-affinity dye, was consistent with the goal of focusing on steady-state conditions and obtaining reliable data on the redistribution of calcium from the rest to a stable repetitive release. As previously reported,^{4,5,40} during a train of stimuli, the amount of calcium released undergoes a progressive change (reduction) of amplitude, and after a few stimuli, a steady state is achieved. The use of a high-affinity, slow dye implies that the impact of lack of PV on the rising and decay phases of the transients could not be reliably analyzed.

The experimental data were analyzed with a mathematical model which simulates half sarcomere with a rotational symmetry, in this respect similar to those proposed by others^{4,41} but sharing with the model of Rincón et al.⁵ a novel and important aspect, that is, the presence of mitochondria, which was neglected in previous models.

The modeling of the mitochondria includes three steps according to the following equation¹⁴:

$$\frac{d[Ca]_{mito}}{dt} = J_{MCU} - J_{NCLX} - J_{buffer}$$

The recent finding by Launikonis laboratory^{9,42} provided evidence of a buffering ability of muscle mitochondria in the order of 1:5000 to 1:10000, consistent with the findings of Chalmers and Nicholls²⁴ on liver and heart mitochondria. The high buffering power can find a molecular basis in the presence of phosphate in the matrix's alkaline environment (see for a review⁸). Following the modeling of Bazil and colleagues,²⁵ we assumed a non-linear biphasic buffer of the mitochondrial matrix. This is an essential point as it implies that, due to the higher peak of mitochondrial calcium reached during the tetanic stimulation in PV-KO compared to WT, the contribution of mitochondria to the distribution of calcium release is lower in WT and becomes much higher in PV-KO (see Table 2). Interestingly, the J_{MCU} predicted by the model corresponds quite well with that measured using a completely different approach than in previous studies.^{28,29} It is, however, higher than the values obtained by other groups²⁷ and predicted by Rincón and colleagues.⁵

The increased calcium distribution in favor of mitochondria in PV-KO fibers should not imply a change in

the total calcium content of the fibers. The main component of the total calcium content at rest is the SR,^{43,44} see also Table 2. Here, with two distinct protocols aimed to cause a complete depletion, we could not show that significant variations occurred in the total calcium content (see Figure S4). Moreover, the unchanged values of free SR calcium and the abundance of the main proteins involved in SR (shown by Butera and colleagues 2021) supported the view that the main storage of calcium was unchanged.

Additionally, we evaluate the contribution of exchange with extra-cellular space (ECS), to explore if the calcium not bound in the absence of PV could have extruded via NCX/PMCA. We found evidence of a potentially more significant exchange based on the greater presence of CEU structures and an increased Mn^{2+} quenching rate (Figure 4). However, such an increase (less than two folds) was not sufficient to compensate for the lack of PV. A further test based on removing ECS calcium did not provide evidence in favor of a significant exchange with ECS.

Thus, mitochondria remove much more calcium from the cytosol and contribute significantly to controlling cytosolic calcium in the fast fibers deprived of PV. This conclusion acquires significant value when seen from the broader perspective of the role of mitochondria in skeletal muscle fibers. As in other cell types, mitochondria do not only play their main role of powerhouse of the cell, but using the term proposed some years ago,⁴⁵ they represent the hub of signaling, regulating apoptosis, and contributing to modulating cell size. Our present data contribute to understanding their role in controlling cytosolic calcium under specific conditions.

4 | MATERIALS AND METHODS

4.1 | Animals

We used (2–3 months old) male C57/BL6J (WT) and $PV^{-/-}$ (PV-KO) mice in all protocols. PV-KO mice were generated as previously described.^{15,31} All procedures were performed under the Italian law D. L. n.26/2014 and approved by the Committee on the Ethics of Animal Experiments of the University of Padova (Permit Number: 666/2018PR). For each group (WT and PV-KO), 6 mice were used for Fura-2 experiments, three mice for Fura-2 fluorescence quenching with Mn^{2+} , eight mice for total calcium analysis (releasing cocktail and caffeine). Six mice were used for inhibitor experiments and eight for silencing, three mice were used for oxygen consumption rate measurements, six mice for calcium retention capacity experiment, six for mitochondrial

cameleon transfection, seven for SR cameleon transfection, and five for contraction experiments on FDB.

4.2 | Ex vivo experiments

Mice were euthanized by cervical dislocation. FDB muscles were dissected while submerged in Krebs Ringer Buffer (KRB—[mM] 120 NaCl, 25 NaHCO₃, 4.7 KCl, 2.5 CaCl₂, 3.15 MgCl₂, 1.3 NaH₂PO₄, 11 glucose, pH 7.4) solution. The muscles were tied to a force transducer (KG Scientific Instruments, Heidelberg, Germany) and a micromanipulator and immersed in KRB solution bubbled with 5% CO₂ and 95% O₂ at 25°C. Supramaximal electrical pulses (1 ms duration) were delivered with a Grass S48 stimulator. The muscle length was adjusted to produce the highest twitch force.

4.3 | FDB electroporation

Electroporation of plasmids in FDB muscle fibers was carried out while the animals were anesthetized with an intraperitoneal injection of Zoletil–Sedaxilan mixture 15 mg/kg. Hyaluronidase solution (2 mg/mL) (Sigma) was injected under the hind limb footpads, and either 10 or 20 µg of plasmid DNA was injected after 30 min. Ten minutes later, muscles were electroporated by applying 20 pulses of 100 V, 20 ms duration, and 1 s interval.

4.4 | FDB dissociation and culture

FDB fiber enzymatic dissociation and culture were performed as previously described.^{15,37} Plated single fibers were electrically stimulated via platinum electrodes in the presence of 50–100 µM N-benzyl-P-toluene-sulfonamide (BTS) at 25°C. Electrical pulses (1 ms duration) at 0.5 Hz for 5 min, then trains of 2 s duration and 60 Hz frequency were delivered with a Grass S88 Square Pulse Stimulator.

4.5 | Sarcoplasmic reticulum and mitochondrial-free Ca²⁺ measurement in FDB fibers

FDB muscles were transfected with plasmids encoding either 4mtD3cpv cameleon targeted to the mitochondrial matrix via a sequence from subunit VIII of human cytochrome c oxidase (COX) or encoding SR-targeted cameleon D1ER carrying a calreticulin peptide sequence. Seven days after transfection fibers were dissociated, plated, and placed on the stage of an inverted fluorescence

microscope (Eclipse-Ti, Nikon Instruments, Amsterdam, Netherlands) at 20X magnification equipped with the perfect focus system. Two images corresponding to YFP (acceptor) and CFP (donor) light emissions were collected with 9 ms resolution time with a cooled CCD camera (C9100-13, Hamamatsu) as previously described.^{7,37} FRET was quantified using ImageJ software. YFP and CFP intensities were corrected for background, and the ratio (*R*) was defined as follows: $R = (\text{YFP fiber} - \text{YFP background}) / (\text{CFP fiber} - \text{CFP background})$.

4.6 | Cytosolic-free Ca²⁺ measurement in FDB fibers

FDB fibers enzymatically dissociated and plated (see above) were loaded with 2 µM Fura-2/AM (Thermo Fisher Scientific) diluted in KRB containing 0.02% pluronic acid F68 (Sigma-Aldrich) for 20 min at 37°C and then washed for 15 min with KRB containing 75 µM BTS (Sigma-Aldrich) to minimize fiber contraction. Calcium release was induced at 25°C with supramaximal electrical pulses (1 ms duration) via platinum electrodes. A dual-beam excitation fluorescence photometry setup (IonOptix Corp.), mounted on a Nikon Eclipse TS100, and equipped with a Xenon Short Arc Lamp, recorded Fura-2 emission light at 510 nm (sampling rate 1 kHz). The free Ca²⁺-concentration levels were inferred from the emission ratio R_{cyto} with excitation at 360 nm and 380 nm.

4.7 | Fura-2 quenching with manganese

FDB fibers loaded with Fura-2 were fully depleted by incubation with two SERCA pump inhibitors (1 µM thapsigargin [Thermo Fisher Scientific, TG]; 15 µM CPA). BTS was added to prevent motion artifacts.⁴⁶ Store-depleted fibers were then bathed in a Ca²⁺-free medium. Fura-2 was excited at 360 nm (isosbestic wavelength), and emission was detected at 510 nm. After recording an initial baseline rate of Fura-2 decay (R_{baseline}), fibers were exposed to Ca²⁺-free medium with 0.5 mM MnCl₂. The maximum rate of decline in Fura-2 fluorescence in the presence of Mn²⁺ (R_{max}) was measured and the rate of SOCE (R_{SOCE}) was calculated as $R_{\text{SOCE}} = R_{\text{max}} - R_{\text{baseline}}$.

4.8 | Transmission electron microscopy

Muscle samples were fixed with 3.5% glutaraldehyde in 0.1 M NaCaCO buffer (pH 7.4), at room temperature and kept at 4°C in fixative until further use. Fixed muscles were post-fixed in osmium tetroxide, stained en-bloc,

embedded, and sectioned as previously described.^{47,48} Ultrathin sections (~50 nm) were then stained for EM in uranyl acetate replacement and lead citrate and examined with a Morgagni Series 268D electron microscope (FEI Company, Brno, Czech Republic) equipped with Megaview III digital camera (Olympus equipped with Soft Imaging System) at 60 kV. The number of CRU was determined in longitudinal sections at 14.000X of magnification, percentage of fibers presenting SR-stacks, number of SR-stacks per area of section, and total extension of the transverse tubule (TT) were measured in transverse sections at 28.000X of magnification. In each sample, 10 fibers were analyzed, and in each fiber, five micrographs were randomly collected from non-overlapping regions.

4.9 | Mathematical model and data simulation

The compartmental model simulates the temporal variation of the Ca^{2+} concentrations in the three main compartments (cytosol, SR, and mitochondria) and buffers through a numerical implementation in MATLAB® (R2021a) available at https://github.com/lorenzomarcucci/ParvalbuminKO_calcium_diffusion. The differential equations, described in the text and in the supplementary information, are solved using the built-in ode15s solver, with initial conditions respecting the steady state in the resting conditions, based on the parameters defined in Table S1.

4.10 | Statistical analysis

Data were expressed as means \pm standard deviation except when differently indicated. The threshold for significance was set $P < 0.05$. An unpaired t-test was used in ex vivo analyses, mitochondrial and SR cameleons, and Fura-2 analyses. Multiple unpaired t-test was used for force-frequency statistical analysis. The comparison in the presence and absence of extracellular calcium for the silencing and for the inhibitor was based on a parametric 2-way ANOVA test with multiple comparison (Fisher's least significant difference test.). Normality tests were performed for each experiment. All data satisfy the Kolmogorov-Smirnov normality test. All the statistical analyses were made with GraphPad Prims® 9.

AUTHOR CONTRIBUTIONS

Lorenzo Marcucci: Conceptualization; software; data curation; investigation; validation; formal analysis; supervision; funding acquisition; visualization; project

administration; resources; writing – original draft; writing – review and editing; methodology. **Leonardo Nogara:** Writing – original draft; data curation; investigation; formal analysis; methodology. **Marta Canato:** Investigation; formal analysis; data curation; methodology. **Elena Germinario:** Investigation; formal analysis; data curation; methodology. **Anna Raffaello:** Investigation; writing – original draft; formal analysis; data curation; methodology. **Michela Carraro:** Investigation; writing – original draft; formal analysis; data curation; methodology. **Paolo Bernardi:** Writing – original draft; methodology. **Laura Pietrangelo:** Investigation; writing – original draft; methodology; formal analysis; data curation. **Simona Boncompagni:** Investigation; writing – original draft; methodology; formal analysis; data curation. **Feliciano Protasi:** Investigation; writing – original draft; methodology; formal analysis; data curation. **Nazareno Paolucci:** Investigation; writing – original draft; methodology; writing – review and editing; formal analysis; data curation. **Carlo Reggiani:** Conceptualization; investigation; writing – original draft; writing – review and editing; methodology; validation; visualization; software; formal analysis; project administration; data curation; supervision; resources.

ACKNOWLEDGMENTS

We thank Professor Beat Schwaller for providing the $\text{PV}^{-/-}$ mice and Professor Livio Finos for his suggestions about the statistical interpretation of part of the data. We also thank Dr. Donato D'Angelo, Dr. Gaia Butera, and Prof. Denis Vecellio Reane for their precious help with genotyping and protein analysis. LM acknowledges the CINECA award under the ISCRA initiative for providing high-performance computing resources and support in the project HP10C78T6R. Open access publishing facilitated by Universita degli Studi di Padova, as part of the Wiley - CRUI-CARE agreement.

FUNDING INFORMATION

This work was funded by the European Union via the Horizon 2020 Research and Innovation Programme under the Marie Skłodowska-Curie grant agreement no. 886232 to L. M., by the Italian Telethon Association (GGP16026) to AR, the Italian Ministry of Health (GR-2016-02362779) to AR, by the Italian Ministry of University and Scientific Research (PRIN 20207P85MH) to AR, by GGP19231 from the Italian Telethon ONLUS to FP, and by subcontract of AR059646 from the National Institutes of Health USA to FP.

CONFLICT OF INTEREST STATEMENT

The authors declare no conflict of interests.

DATA AVAILABILITY STATEMENT

The data generated and analyzed during this study are included in this article. Supplementary data supporting this study's findings and the Matlab® code for the simulations are available from the corresponding author upon request. The code is also available at https://github.com/lorenzomarcucci/ParvalbuminKO_calcium_diffusion.

ORCID

Lorenzo Marcucci  <https://orcid.org/0000-0002-9542-4417>

REFERENCES

- Bolaños P, Calderón JC. Excitation-contraction coupling in mammalian skeletal muscle: blending old and last-decade research. *Front Physiol.* 2022;13:989796.
- Heizmann CW, Berchtold MW, Rowlerson AM. Correlation of parvalbumin concentration with relaxation speed in mammalian muscles. *Proc Natl Acad Sci USA.* 1982;79(23):7243-7247.
- Füchtbauer EM, Rowlerson AM, Götz K, et al. Direct correlation of parvalbumin levels with myosin isoforms and succinate dehydrogenase activity on frozen sections of rodent muscle. *J Histochem Cytochem.* 1991;39(3):355-361.
- Baylor SM, Hollingworth S. Simulation of Ca^{2+} movements within the sarcomere of fast-twitch mouse fibers stimulated by action potentials. *J Gen Physiol.* 2007;130(3):283-302.
- Rincón OA, Milán AF, Calderón JC, Giraldo MA. Comprehensive simulation of Ca^{2+} transients in the continuum of mouse skeletal muscle fiber types. *Int J Mol Sci.* 2021;22(22):12378.
- Rudolf R, Mongillo M, Magalhães PJ, Pozzan T. In vivo monitoring of Ca^{2+} uptake into mitochondria of mouse skeletal muscle during contraction. *J Cell Biol.* 2004;166(4):527-536.
- Scorzeto M, Giacomello M, Toniolo L, et al. Mitochondrial Ca^{2+} -handling in fast skeletal muscle fibers from wild type and calsequestrin-null mice. *PLoS One.* 2013;8(10):e74919.
- Garbincius JF, Elrod JW. Mitochondrial calcium exchange in physiology and disease. *Physiol Rev.* 2022;102(2):893-992.
- Lamboleay CR, Pearce L, Seng C, et al. Ryanodine receptor leak triggers fiber Ca^{2+} redistribution to preserve force and elevate basal metabolism in skeletal muscle. *Sci Adv.* 2021;7(44):eabi7166.
- Marcucci L, Michelucci A, Reggiani C. Cytosolic Ca^{2+} gradients and mitochondrial Ca^{2+} uptake in resting muscle fibers: a model analysis. *Biophys Rep.* 2023;3(3):100117.
- Díaz-Vegas A, Eisner V, Jaimovich E. Skeletal muscle excitation-metabolism coupling. *Arch Biochem Biophys.* 2019;664:89-94.
- Mammucari C, Gherardi G, Zamparo I, et al. The mitochondrial calcium uniporter controls skeletal muscle trophism in vivo. *Cell Rep.* 2015;10(8):1269-1279.
- Li A, Yi J, Li X, Zhou J. Physiological Ca^{2+} transients versus pathological steady-state Ca^{2+} elevation, who flips the ROS coin in skeletal muscle mitochondria. *Front Physiol.* 2020;11:595800.
- Reggiani C, Marcucci L. A controversial issue: can mitochondria modulate cytosolic calcium and contraction of skeletal muscle fibers? *J Gen Physiol.* 2022;154(9):e202213167.
- Butera G, Vecellio Reane D, Canato M, et al. Parvalbumin affects skeletal muscle trophism through modulation of mitochondrial calcium uptake. *Cell Rep.* 2021;35(5):109087.
- Marcucci L, Canato M, Protasi F, Stienen GJM, Reggiani C. A 3D diffusional-compartmental model of the calcium dynamics in cytosol, sarcoplasmic reticulum and mitochondria of murine skeletal muscle fibers. *PLoS One.* 2018;13(7):e0201050.
- Chen G, Carroll S, Racay P, et al. Deficiency in parvalbumin increases fatigue resistance in fast-twitch muscle and upregulates mitochondria. *Am J Physiol Cell Physiol.* 2001;281(1):C114-C122.
- Chen G, Racay P, Bichet S, Celio MR, Eggl P, Schwaller B. Deficiency in parvalbumin, but not in calbindin D-28k upregulates mitochondrial volume and decreases smooth endoplasmic reticulum surface selectively in a peripheral, subplasmalemmal region in the soma of Purkinje cells. *Neuroscience.* 2006;142(1):97-105.
- Michelucci A, Boncompagni S, Pietrangelo L, et al. Transverse tubule remodeling enhances Orail-dependent Ca^{2+} entry in skeletal muscle. *elife.* 2019;8:e47576.
- Di Marco G, Vallese F, Jourde B, et al. A high-throughput screening identifies MICU1 targeting compounds. *Cell Rep.* 2020;30(7):2321-2331.e6.
- Boncompagni S, Michelucci A, Pietrangelo L, Dirksen RT, Protasi F. Exercise-dependent formation of new junctions that promote STIM1-Orail assembly in skeletal muscle. *Sci Rep.* 2017;7(1):14286.
- Favaron M, Bernardi P. Tissue-specific modulation of the mitochondrial calcium uniporter by magnesium ions. *FEBS Lett.* 1985;183(2):260-264.
- Blomeyer CA, Bazil JN, Stowe DF, Dash RK, Camara AKS. Mg^{2+} differentially regulates two modes of mitochondrial Ca^{2+} uptake in isolated cardiac mitochondria: implications for mitochondrial Ca^{2+} sequestration. *J Bioenerg Biomembr.* 2016;48(3):175-188.
- Chalmers S, Nicholls DG. The relationship between free and total calcium concentrations in the matrix of liver and brain mitochondria. *J Biol Chem.* 2003;278(21):19062-19070.
- Bazil JN, Blomeyer CA, Pradhan RK, Camara AKS, Dash RK. Modeling the calcium sequestration system in isolated guinea pig cardiac mitochondria. *J Bioenerg Biomembr.* 2013;45(3):177-188.
- Boncompagni S, Rossi AE, Micaroni M, et al. Mitochondria are linked to calcium stores in striated muscle by developmentally regulated tethering structures. *Mol Biol Cell.* 2009;20(3):1058-1067.
- Sembrowich WL, Quintinskie JJ, Li G. Calcium uptake in mitochondria from different skeletal muscle types. *J Appl Physiol (1985).* 1985;59(1):137-141.
- Fieni F, Lee SB, Jan YN, Kirichok Y. Activity of the mitochondrial calcium uniporter varies greatly between tissues. *Nat Commun.* 2012;3:1317.
- Yi J, Ma C, Li Y, et al. Mitochondrial calcium uptake regulates rapid calcium transients in skeletal muscle during excitation-contraction (E-C) coupling. *J Biol Chem.* 2011;286(37):32436-32443.
- Fukutani A, Westerblad H, Jardemark K, Bruton J. Ca^{2+} and force during dynamic contractions in mouse intact skeletal muscle fibers. *Sci Rep.* 2024;14(1):689.

31. Schwaller B, Dick J, Dhoot G, et al. Prolonged contraction-relaxation cycle of fast-twitch muscles in parvalbumin knock-out mice. *Am J Phys.* 1999;276(2):C395-C403.
32. Raymackers JM, Gailly P, Schoor MC, et al. Tetanus relaxation of fast skeletal muscles of the mouse made parvalbumin deficient by gene inactivation. *J Physiol.* 2000;527(Pt 2):355-364.
33. Tarpey MD, Amorese AJ, Balestrieri NP, et al. Characterization and utilization of the flexor digitorum brevis for assessing skeletal muscle function. *Skelet Muscle.* 2018;8(1):14.
34. Petro JL, Milán AF, Arenas E, Valle L, Hernández V, Calderón JC. Intact short, intermediate, and long skeletal muscle fibers obtained by enzymatic dissociation of six hindlimb muscles of mice: beyond flexor digitorum brevis. *J Vis Exp.* 2023;202:e65851. doi:10.3791/65851
35. Murgia M, Nagaraj N, Deshmukh AS, et al. Single muscle fiber proteomics reveals unexpected mitochondrial specialization. *EMBO Rep.* 2015;16(3):387-395.
36. Palmer AE, Tsien RY. Measuring calcium signaling using genetically targetable fluorescent indicators. *Nat Protoc.* 2006;1(3):1057-1065.
37. Canato M, Scorzeto M, Giacomello M, Protasi F, Reggiani C, Stienen GJM. Massive alterations of sarcoplasmic reticulum free calcium in skeletal muscle fibers lacking calsequestrin revealed by a genetically encoded probe. *Proc Natl Acad Sci USA.* 2010;107(51):22326-22331.
38. Canato M, Capitanio P, Cancellara L, et al. Excessive accumulation of Ca²⁺ in mitochondria of Y522S-RYR1 knock-in mice: a link between leak from the sarcoplasmic reticulum and altered redox state. *Front Physiol.* 2019;10:1142.
39. Palmer AE, Giacomello M, Kortemme T, et al. Ca²⁺ indicators based on computationally redesigned calmodulin-peptide pairs. *Chem Biol.* 2006;13(5):521-530.
40. Calderón JC, Bolaños P, Caputo C. Tetanic Ca²⁺ transient differences between slow- and fast-twitch mouse skeletal muscle fibres: a comprehensive experimental approach. *J Muscle Res Cell Motil.* 2014;35(5-6):279-293.
41. Cannell MB, Allen DG. Model of calcium movements during activation in the sarcomere of frog skeletal muscle. *Biophys J.* 1984;45(5):913-925.
42. Gaglianone RB, Launikonis BS. Muscle fibre mitochondrial [Ca²⁺] dynamics during Ca²⁺ waves in RYR1 gain-of-function mouse. *Acta Physiol (Oxf).* 2024;240(3):e14098.
43. Fryer MW, Stephenson DG. Total and sarcoplasmic reticulum calcium contents of skinned fibres from rat skeletal muscle. *J Physiol.* 1996;493(Pt 2):357-370.
44. Lamboley CRH, Kake Guena SA, Touré F, et al. New method for determining total calcium content in tissue applied to skeletal muscle with and without calsequestrin. *J Gen Physiol.* 2015;145(2):127-153.
45. Szabadkai G, Duchen MR. Mitochondria: the hub of cellular Ca²⁺ signaling. *Physiology (Bethesda).* 2008;23:84-94.
46. Wei-LaPierre L, Carrell EM, Boncompagni S, Protasi F, Dirksen RT. Orai1-dependent calcium entry promotes skeletal muscle growth and limits fatigue. *Nat Commun.* 2013;4(1):2805.
47. Pietrangelo L, D'Incecco A, Ainbinder A, et al. Age-dependent uncoupling of mitochondria from Ca²⁺ release units in skeletal muscle. *Oncotarget.* 2015;6(34):35358-35371.
48. Pietrangelo L, Michelucci A, Ambrogini P, et al. Muscle activity prevents the uncoupling of mitochondria from Ca²⁺ release units induced by ageing and disuse. *Arch Biochem Biophys.* 2019;663:22-33.

SUPPORTING INFORMATION

Additional supporting information can be found online in the Supporting Information section at the end of this article.

How to cite this article: Marcucci L, Nogara L, Canato M, et al. Mitochondria can substitute for parvalbumin to lower cytosolic calcium levels in the murine fast skeletal muscle. *Acta Physiol.* 2024;240:e14208. doi:10.1111/apha.14208